Journal of Solid State Chemistry 184 (2011) 1915–1923

Contents lists available at ScienceDirect

Journal of Solid State Chemistry

journal homepage: www.elsevier.com/locate/jssc

TPR investigations on the reducibility of Cu supported on Al_2O_3, zeolite Y and SAPO-5

Dang Lanh Hoang*, Thi Thuy Hanh Dang, Jana Engeldinger, Matthias Schneider, Jörg Radnik, Manfred Richter, Andreas Martin

Leibniz-Institut für Katalyse e.V. an der Universität Rostock, Albert-Einstein-Str. 29a, D-18059 Rostock, Germany

ARTICLE INFO

Article history:
Received 2 February 2011
Received in revised form
12 May 2011
Accepted 29 May 2011
Available online 6 June 2011

Keywords:
TPR
Cu reducibility
Cu oxidation state
Cu/Al_2O_3
Cu/Y
Cu/SAPO-5

ABSTRACT

Reducibility of Cu supported on Al_2O_3, zeolite Y and silicoaluminophosphate SAPO-5 has been investigated in dependence on the Cu content using a method combining conventional temperature programmed reduction (TPR) by hydrogen with reoxidation in N_2O followed by a second the so-called surface-TPR (s-TPR). The method enables discrimination and a quantitative estimation of the Cu oxidation states +2, +1 and 0. The quantitative results show that the initial oxidation state of Cu after calcination in air at 400 °C, independent on the nature of the support, is predominantly +2. Cu^{2+} supported on Al_2O_3 is quantitatively reduced by hydrogen to metallic Cu^0. Comparing the TPR of the samples calcined in air and that of samples additionally pre-treated in argon reveals that in zeolite Y and SAPO-5 Cu^{2+} cations are stabilized as weakly and strongly forms. In both systems, strongly stabilized Cu^{2+} ions are not auto-reduced by pre-treatment in argon at 650 °C, but are reduced in hydrogen to form Cu^+. The weakly stabilized Cu^{2+} ions, in contrast, may be auto-reduced by pre-treatment in argon at 650 °C forming Cu^+ but are reduced in hydrogen to metallic Cu^0.

1. Introduction

The reducibility of Cu is one of the most significant characteristics of Cu containing catalysts, which are intensively used in a variety of chemical processes. Among the well known methods for studying the reducibility of Cu, such as XPS, FTIR, EPR, EXAFS etc., the temperature programmed reduction (TPR) using hydrogen as a reducing agent is a straightforward method and has been widely applied [1–5]. The advantages of TPR consist in the possibility to record the copper reduction process in dependence on temperature and to allow a quantification of reducible Cu species on non-reducible supports, e.g. [4–14]. Moreover, a novel method reported by e.g. Sato et al. [15] that combines TPR measurement with selective reoxidation by N_2O at low temperature enables the distinction between bulk and surface Cu^0. The Cu dispersion and the metal surface of Cu supported on different oxides or oxide mixtures, e.g. MgO, SiO_2 and Al_2O_3 [15] or SiO_2–TiO_2 and SiO_2–ZrO_2, [16] can be, therefore, calculated. Actually, this could be performed since the N_2O treatment at 30–50 °C was shown to reoxidize exclusively surface Cu^0 of metallic clusters to Cu^+ [15,16]. In a TPR carried out after the N_2O reoxidation (the so-called s-TPR [16]), the amounts of hydrogen consumed for reduction of Cu^+ formed after such N_2O reoxidation would correspond to the portion of exposed surface Cu^0. The ratio of the exposed surface Cu^0 to the total Cu is defined as Cu dispersion, based on which the Cu metal surface area per unit weight of catalyst can be estimated [15–17]. The theoretical and experimental aspects of the combination between TPR and N_2O oxidation of Cu supported on oxides or oxide mixtures were examined in detail by Sato et al. [15].

Cu containing silicoaluminophosphate (SAPO) molecular sieves, as known, may be used as catalysts for numerous relevant reactions [18–20]. However, questions concerning the nature of Cu, including, e.g. location as well as its reducibility, have only scarcely been investigated for Cu-modified SAPO-*n* (where *n* symbolizes the structure type of material), and the catalytic role of different Cu species of these materials is still a matter of discussion [18]. Of course, before the catalytic roles of different Cu species could be uncovered, one of the most important problems is, once more, the distinction and the quantitative evaluation of Cu in different valence states. In this paper, therefore, the combination of the conventional TPR and the s-TPR technique is applied for the first time aiming at investigating the oxidation states of Cu supported on SAPO-5, i.e. Cu/SAPO-5. XRD and XPS measurements were partially performed for affirming the conclusions drawn from TPR. Since the TPR method has been already used for investigating the reducibility of Cu supported on zeolite Y, i.e. Cu/Y, or on alumina, i.e. Cu/Al_2O_3 (e.g. [1–3,6–8,12,21,22]), these materials, as references, were also prepared and measured by TPR combined with s-TPR.

* Corresponding author. Fax: +49 381 1281 51277.
E-mail address: Dang-Lanh.Hoang@catalysis.de (D.L. Hoang).

0022-4596/$ - see front matter © 2011 Elsevier Inc. All rights reserved.
doi:10.1016/j.jssc.2011.05.042

2. Experimental section

2.1. Supports

An alumina, γ-Al_2O_3, a zeolite Y in ammonium form, NH_4-Y (Si/Al=2.3), and a silicoaluminophosphate material, SAPO-5 (Al/P/Si=1.00/0.94/0.07), were used as supports for copper. γ-Al_2O_3 and NH_4-Y were commercial products, supplied by Merck and Zeolyst International, respectively. SAPO-5 has been synthesized by the method described in [23]. Before using them, Al_2O_3 was calcined in an air flow (200 mL/min) at 400 °C for 10 h to eliminate moisture and the synthesized SAPO-5 was calcined in an air flow (200 mL/min) at 550 °C for 12 h to remove the template. In order to avoid the dealumination of zeolite, NH_4-Y was dried at 120 °C overnight and used without any further pre-treatment.

Specific surface areas (BET) of the supports were determined by nitrogen adsorption at -196 °C applying the ASAP 2010 characterization unit (Micromeritics). Before N_2 adsorption, the samples were evacuated (0.13 Pa) in situ at 400 °C for 4 h.

The total acidities (mmol NH_3/g) of the commercial alumina and the synthesized SAPO-5 were determined by temperature-programmed desorption of ammonia (TPDA), which was carried out in a home-made apparatus consisting of a gas flow system, a high temperature oven and a quartz reactor. The samples were treated in air at 550 °C for 0.5 h to remove moisture and cooled down to 100 °C in He of high purity (6.0) prior to NH_3 adsorption, which was carried out at 100 °C for 0.5 h in a flow of He containing 5% NH_3. Afterwards TPDA experiments were carried out from 100 to 600 °C in He flow (50 cm^3 min^{-1}) with a heating rate of 10 K/min. Desorption of NH_3 was monitored and evaluated by a thermal conductivity detector, TCD (GOW-Mac Instrument Co.), which was calibrated by performing thermal decomposition of varying amounts of manganese ammonium phosphate.

The total acidity of NH_4-Y was determined by its temperature-programmed decomposition (TPDec) performed in the same apparatus in a He flow with a heating rate of 10 K/min from room temperature up to 600 °C. The concentration of ammonia released was recorded and evaluated in the way described above.

2.2. Catalyst preparation

The Cu/SAPO-5 samples were prepared by incipient wetness impregnation of the template-free SAPO-5 with $Cu(NO_3)_2 \cdot 6H_2O$ (Sigma-Aldrich) solutions containing the appropriate amount of Cu for loading of ca. 0.8–9.2 wt%. The amounts of solution were appropriately chosen to achieve a complete wetness of material powder by the liquid. The Cu/Al_2O_3 and Cu/Y reference samples were also prepared by incipient wetness method. The powder of the γ-Al_2O_3 and NH_4-Y zeolite supports were impregnated with $Cu(NO_3)_2 \cdot 6H_2O$ solutions containing the appropriate amount of Cu for loading of ca. 2–15 wt%. The impregnated powders were dried overnight at 120 °C, compacted and crushed for appropriate particle size (0.3–0.7 mm) and then calcined in an air flow at 400 °C for 5 h. The calcined samples will be denominated as (*x*)Cu/S where *x* denotes the Cu content determined by ICP (wt%), and S the support type (Al_2O_3, Y and SAPO-5). Before TPR experiments, a portion of each calcined material was additionally pre-treated by heating it in a dry argon flow (25 mL/min) from 25 to 650 °C (heating rate= 2 K/min) and keeping the sample at this temperature for 8 h. This pre-treatment resembles the one used for activating chloride-free Cu/Y catalysts in oxidative gas phase carbonylation of methanol to dimethylcarbonate [12,13]. In analogy, the pre-treatment in argon will be denoted in this paper as activation as well, and samples will be designated as (*x*)Cu/S-(act) where *x* and S, again, denote the Cu content and the kind of support, respectively, and (act) indicates the additional pre-treatment in argon at 650 °C.

2.3. Characterization

The reducibility of Cu species supported on γ-Al_2O_3, Y and SAPO-5 was investigated by means of TPR. The valence states of Cu on (*6.53*)Cu/SAPO-5 and (*6.53*)Cu/SAPO-5-(act) as representative samples were additionally examined by XRD and XPS.

TPR was performed using a gas flow system described in detail elsewhere [24]. The material was calcined once more in situ at 400 °C in an air flow for 0.5 h and then cooled down to 50 °C in a dried nitrogen flow before the TPR experiment. The (*x*)Cu/S-(act) samples were again treated in situ in an argon flow directly before the TPR experiment at 650 °C for 0.5 h to avoid any air effects. These TPR experiments will be denoted as TPR-(act). The procedure of TPR experiments consists of different steps performed in sequence:

(i) the conventional TPR or TPR-(act),
(ii) the reoxidation in a He flow containing 10% N_2O at 50 °C for 0.5 h and
(iii) the s-TPR [16] or s-TPR-(act).

As reported in literature, exposed surface Cu^0 species that may be formed during TPR (step (i)) according to reaction (1) and/or (2):

$$CuO + H_2 \rightarrow Cu + H_2O \quad (1)$$

$$Cu_2O + H_2 \rightarrow 2Cu + H_2O \quad (2)$$

would be reoxidized by N_2O at 50 °C to Cu^+ during step (ii) according to reaction (3) [15–17,25–27]:

$$2Cu + N_2O \rightarrow Cu_2O + N_2 \quad (3)$$

During subsequent s-TPR, Cu^+ will be again reduced to Cu^0 according to reaction (2). A consumption of hydrogen during s-TPR would be, therefore, an indication for the existence of surface metallic Cu^0 formed after reduction during TPR. Moreover, based on the hydrogen amount consumed during s-TPR for reducing Cu^+ cations (step (iii)), the portion of exposed surface Cu^0 and therefore, the Cu dispersion as well, can quantitatively be estimated [15–17].

The TPR and s-TPR runs were carried out from 50 to 550 °C in a 5.03 vol% H_2/argon flow at a heating rate of 10 K/min. Optimum sample weights (0.020-0.45 g) corresponding to a reduction in gas flow rate of 15 mL/min had been estimated according to the equation proposed by Monti and Baiker [28]. The quantitative analysis of the TPR results, based on the integration of calibrated hydrogen consumption peak areas, was carried out by the method described elsewhere [24].

For XRD studies, the samples were measured on a STADI P automated transmission diffractometer from STOE (Darmstadt, Germany) with an incident beam curved germanium monochromator selecting Cu$K\alpha_1$ radiation (λ=1.5406 Å) and a 6° linear position sensitive detector (PSD). The alignment was checked by the use of a silicon standard. The data were collected in the 2θ range from 5° to 60° with a step size of 0.5° and a measurement time of 50 s per step. The phase composition of the samples was determined using the program suite WINXPow by STOE&CIE with inclusion of the Powder Diffraction File PDF2 of the International Centre of Diffraction Data (ICDD).

The XPS measurements were performed with an ESCALAB 220iXL (ThermoScientific) using monochromatic Al$K\alpha$ radiation. The binding energies were referred to the C1s peak at 284.8 eV. The spectra were fitted with Gaussian–Lorentzian curves to determine the peak maxima and the areas. The concentrations of the elements in the near-surface region were obtained after division by the element-specific Scofield factors and the transmission function of the spectrometer.

3. Results

3.1. Support characteristics

The TPDA profiles of SAPO-5 and Al_2O_3 as well as the TPDec of NH_4-Y are depicted in Fig. 1A and B, respectively. As known, peak positions on the temperature axis during TPDA represent the acid strength of sites whereas the peak areas correspond to the acid site concentration [29]. The same can be applied to the TPDec profiles. The TPDA profiles in Fig. 1 reveal the clear differences concerning the strength of acid sites of the supports used. Namely, Al_2O_3 desorbs NH_3 in a wide temperature range showing a small peak with a maximum at T_{max}=ca. 170–180 °C and an expanded tail of low intensities at higher temperatures. With SAPO-5 and NH_4-Y, the corresponding TPDA and TPDec profiles consist of the peaks at 190 and 212 °C, respectively, and at least one peak at higher temperatures, ca. 300 and 400 °C, respectively. The low temperature (LT) peaks, as known [29], are believed to be caused by desorption of NH_3 from weak acid sites and the high temperature (HT) peaks by desorption of NH_3 bonded to strong acid sites. The acid sites on alumina are surely of Lewis nature but the ones on zeolite Y and SAPO-5 consist of both Lewis and Brønsted sites [30,31]. So, as appeared, the profiles shown in Fig. 1 evidence the existence of strong acid sites on zeolite Y and silicoaluminophosphate SAPO-5 materials as well as even in minor concentrations on alumina. Moreover, based on the positions of HT peaks, the strength of the strong acid sites can be arranged in the order zeolite Y > SAPO-5 ≫ Al_2O_3. With zeolite Y and SAPO-5 materials, a formal deconvolution of the TPDA or TPDec profiles by the Gaussian fitting peaks enables the quantitative estimation of the amounts of strong acid sites. The maximum temperatures of NH_3 desorption, the total acidities, the amounts of weak and strong acid sites, the specific surface areas and the pore volumes of the supports are listed in Table 1. It is worth mentioning that a dealumination of zeolite Y always takes place during such thermal treatment as described in Section 2. This leads to a loss of acid sites, and therefore, the acidity obtained for zeolite Y by TPDec is always lower than its real acidity [29]. Based on the obtained values for acidity and assuming that all the acid sites can fix Cu ions, the maximal loading of the Cu as well as the loading of Cu ion fixed by strong acid sites can be calculated, see Table 1. Thus, at first glance it can be noted that the maximal loading of Cu fixed by zeolite Y is clearly greater than the one by SAPO-5.

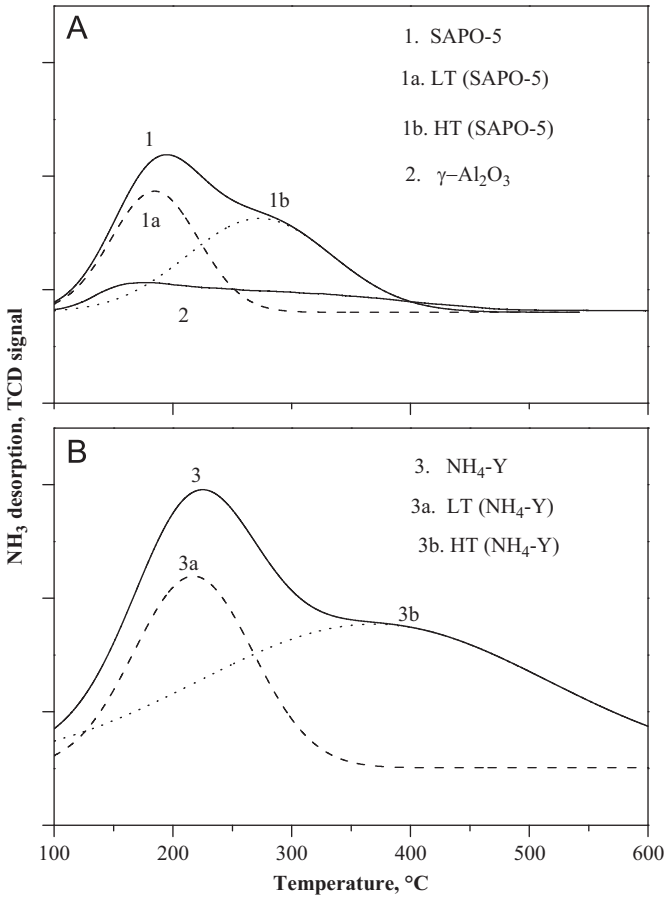

Fig. 1. NH_3-TPD of SAPO-5 and γ-Al_2O_3 (A) and TPDec of NH_4-Y (B) and profile deconvolution by the Gaussian fitting into a low-temperature peak (LT) and a high-temperature peak (HT).

3.2. Cu/Al_2O_3

TPR experiments were carried out on (x)Cu/Al_2O_3 and (x)Cu/Al_2O_3-(act) samples (x=*0, 1.86, 4.80, 6.42, 8.47* and *15.19*). Quantitative TPR and s-TPR results, hydrogen consumptions and the amount of metallic Cu^0 calculated from s-TPR are listed in Table 2. In order to show the influence of the argon pre-treatment at 650 °C on the reduction behavior of Cu supported on γ-Al_2O_3, the TPR, TPR-(act) and s-TPR profiles of samples (*1.86*)Cu/Al_2O_3, (*4.80*)Cu/Al_2O_3, (*8.47*)Cu/Al_2O_3, and (*1.86*)Cu/Al_2O_3-(act), (*4.80*)Cu/Al_2O_3-(act) and (*8.47*)Cu/Al_2O_3-(act) are shown in Fig. 2. The hydrogen consumption profiles exhibit maxima at different temperatures, confirming the existence of various Cu species on γ-Al_2O_3 after standard oxidative pre-treatment. It is also evident that the argon pre-treatment has modified the concentration and nature of Cu species (see Fig. 2). It can be observed that the hydrogen consumptions for reduction of (*1.86*)Cu/Al_2O_3 and (*4.80*)Cu/Al_2O_3 are significantly higher than that for reduction of the corresponding activated samples (*1.86*)Cu/Al_2O_3-(act) and (*4.80*)Cu/Al_2O_3-(act). The s-TPR profiles exhibit hydrogen consumption peaks in the temperature range 75–225 °C, and practically do not differ from the profiles s-TPR-(act) (not shown in Fig. 2).

Fig. 3A depicts the dependence of hydrogen consumption on the Cu content for TPR of (x)Cu/Al_2O_3 and (x)Cu/Al_2O_3-(act) samples.

Table 1
Specific surface area, pore volumes of supports used as well as the maximum temperatures of NH_3 desorption, concentration of acid sites and maximal content of Cu could be fixed.

Materials	Specific surface area (BET) (m^2/g)	Pore volume (cm^3/g)	T_{max} of NH_3 desorption (°C)		Concentration of acid sites (mmol NH_3/g)			Maximal content (wt%) of Cu could be fixed	
			LT	HT	Total	Weak (LT)[a]	Strong (HT)[a]	By all the acid sites	By the strong sites
Zeolite Y	750	0.3	216	380	2.75	0.86	1.89	17.6	12.1
SAPO-5	380	0.16	185	281	1.23	0.56	0.67	7.8	4.2
Al_2O_3	133	0.5	160		0.3	0.3	–[b]	1.9	–

[a] Obtained by the Gaussian fitting.
[b] No reasonable fitting possible, cf. Fig. 1A. The corresponding profiles are presented in Fig. 1.

Table 2
Quantitative TPR results obtained on $(x)Cu/Al_2O_3$ and $(x)Cu/Al_2O_3$-(act).

Cu content (x=wt%) (ICP)	*1.86*	*4.80*	*6.42*	*8.47*	*15.19*
Cu content (mmol/g) (ICP)	*0.29*	*0.76*	*1.01*	*1.33*	*2.39*
Hydrogen consumption experimentally obtained during TPR (mmol H_2/g)	0.29	0.76	1.01	1.34	2.44
Hydrogen consumption experimentally obtained during s-TPR (mmol H_2/g)	0.08	0.21	0.33	0.28	0.15
Exposed surface Cu^0 detected by s-TPR (mmol/g)[a]	0.17	0.43	0.66	0.56	0.30
Hydrogen consumption experimentally obtained during TPR-(act) (mmol H_2/g)	0.17	0.41	0.62	1.21	2.15
Hydrogen consumption experimentally obtained during s-TPR-(act) (mmol H_2/g)	0.08	0.21	0.28	0.22	0.21
Exposed surface Cu^0 detected by s-TPR-(act) (mmol/g)[a]	0.15	0.41	0.57	0.44	0.42
Hydrogen consumption expected for reduction (mmol H_2/g)					
Cu(II) to Cu(0)[b]	0.29	0.76	1.01	1.33	2.39
Cu(II) to Cu(I)[c]	0.15	0.38	0.50	0.67	1.20

[a] According to reaction (2).
[b] According to reaction (1).
[c] According to reaction (5).

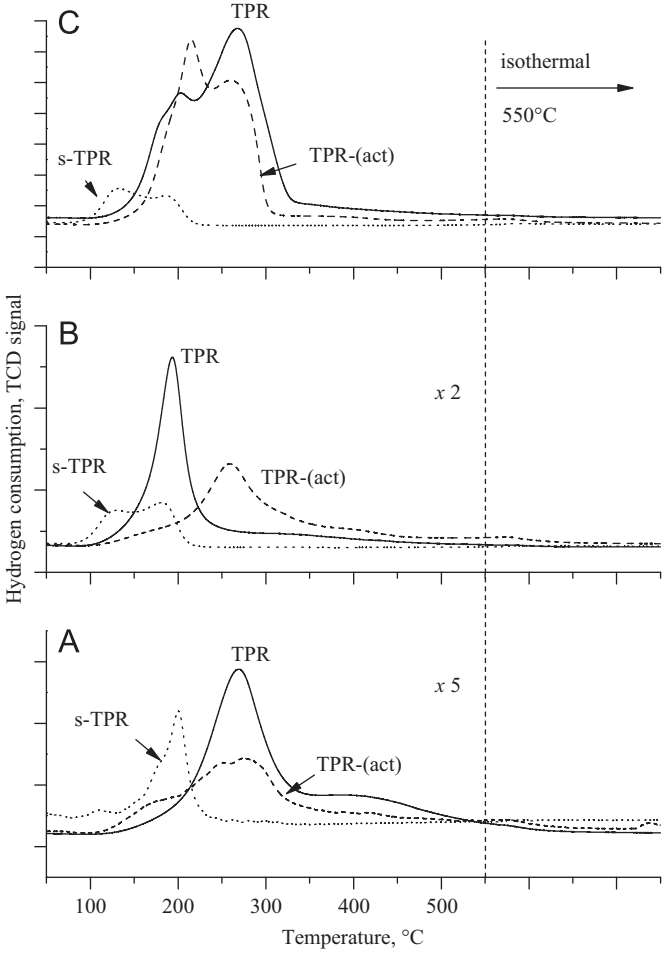

Fig. 2. TPR, TPR-(act) and s-TPR profiles of $(1.86)Cu/Al_2O_3$ (A), $(4.80)Cu/Al_2O_3$ (B) and $(8.47)Cu/Al_2O_3$ (C) samples. (The intensities of TCD signals in (B) and (C) are multiplied by 2 and 5, respectively.)

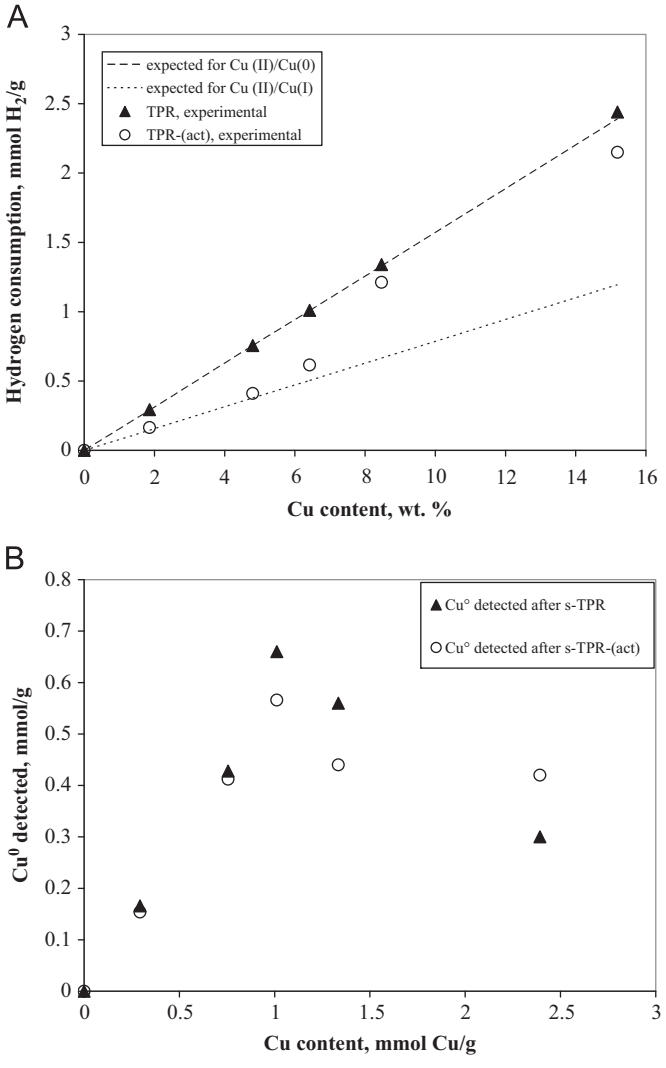

Fig. 3. (A) Hydrogen consumption (mmol H_2/g) obtained by TPR and TPR-(act) in dependence on Cu content (wt%) of Cu/Al_2O_3. (B) Amounts of Cu^0 detected by s-TPR and s-TPR-(act) in dependence on Cu content (wt%) of Cu/Al_2O_3.

The theoretical amounts of the hydrogen consumption expected for a complete reduction of the available Cu^{2+} ions to metallic Cu^0 $(n-m=2)$ or to Cu^+ $(n-m=1)$ according to

$$Cu^{n+} + [(n-m)/2]H_2 \leftrightarrow Cu^{m+} + (n-m)H^+ \quad (4)$$

are included in Fig. 3A as dashed lines. The diagram shows that the total amount of hydrogen consumed during TPR of the $(x)Cu/Al_2O_3$ samples with $x=15.19$ fits the theoretical curve for a change of the Cu oxidation state $n-m=2$, whereas the hydrogen consumption of the $(x)Cu/Al_2O_3$-(act) samples fits the curve for a change of the Cu oxidation state $n-m=1$ up to $x=6.42$. However, at $x>6.42$, the change of oxidation state $n-m=2$ is almost the same for $(x)Cu/Al_2O_3$ and $(x)Cu/Al_2O_3$-(act) samples.

The appearance of hydrogen consumption peaks in the s-TPR profiles, see Fig. 2, evidences the existence of metallic Cu^0 after the first TPR run on $(x)Cu/Al_2O_3$ and $(x)Cu/Al_2O_3$-(act) samples.

The amounts of surface metallic Cu^0 were calculated according to reaction (2) based on the hydrogen consumption during s-TPR and s-TPR-(act), and depicted in Fig. 3B, versus the available Cu amount determined by ICP. As shown, the amounts of surface Cu^0 detected by s-TPR and s-TPR-(act) increase linearly with increase in Cu content up to 1.0 mmol Cu^0/g loading ($x=6.42$). But, with higher Cu contents (>1.0 mmol Cu^0/g), the amount of detected Cu^0 drastically decreased. It is worth mentioning that the ratios of the surface Cu^0 detected by s-TPR or s-TPR-(act) (mmol/g) to Cu total amount (mmol/g) determined by TPR or ICP correspond to the dispersion as defined in [15,16] for Cu supported on metal oxides.

3.3. Cu/Y-zeolite

TPR experiments were carried out on (x)Cu/Y and (x)Cu/Y-(act) samples ($x=$*1.86, 5.31, 8.22, 11.82* and *15.96*). The quantitative TPR results are listed in Table 3. To examine the influence of the argon pre-treatment on the reduction of Cu supported on Y, the TPR profiles of (*1.86*)Cu/Y, (*5.31*)Cu/Y and (*8.22*)Cu/Y are compared with the TPR-(act) profiles of (*1.86*)Cu/Y-(act), (*5.31*)Cu/Y-(act) and (*8.22*)Cu/Y-(act), respectively, in Fig. 4. As appeared, the reduction profiles of Cu/Y samples consist of at least two peaks, an LT peak at a T_{max} of ca. 250 °C and a HT peak at T_{max} 300–500 °C. With increase in Cu loading, the intensities of the LT peaks increase (please note the different scale of the axes), and the T_{max} of the HT peaks is shifted to lower temperatures. The reduction profiles of the (x)Cu/Y-(act) samples show a broad but uniform peak with T_{max} at 300–350 °C, the value of which is slightly shifted to lower temperature with increase in Cu loading as well. Comparing the reduction profiles of the TPR and TPR-(act) it can be concluded that the argon pre-treatment has removed the LT peak almost totally. Moreover, it should be mentioned that the s-TPR and s-TPR-(act) profiles of the samples with $x<8$ (the latter are not shown in Fig. 4) do not give any hydrogen consumption. This proves the absence of surface metallic Cu^0 in these Cu/Y samples after TPR and TPR-(act).

The dependence of hydrogen consumption during TPR and TPR-(act) on the Cu content in the studied Cu/Y samples is depicted in Fig. 5. For convenience, the amounts of the hydrogen consumption expected for a complete reduction of the available Cu^{2+} to metallic Cu^0 ($n-m=2$) or to Cu^+ ($n-m=1$) according to Eq. (4) are included as well. It shows that the total amount of hydrogen consumed during TPR of the samples (x)Cu/Y with $x<8$ fits the theoretical curve for the change of the Cu oxidation state $n-m=1$. At higher Cu loading ($x>8$), the ($n-m$) values increase and approach the value $n-m=2$. Unlike this, the hydrogen consumption of the (x)Cu/Y-(act) samples at $x>8$ deviates from the expected curve for the change of the Cu oxidation state $n-m=1$ values to a curve with $n-m<1$.

3.4. Cu/SAPO-5

The quantitative TPR results of (x)Cu/SAPO-5 and (x)Cu/SAPO-5-(act) samples are summarized in Table 4. The TPR, TPR-(act) and s-TPR profiles of (x)Cu/SAPO-5 as well as (x)Cu/SAPO-5-(act)

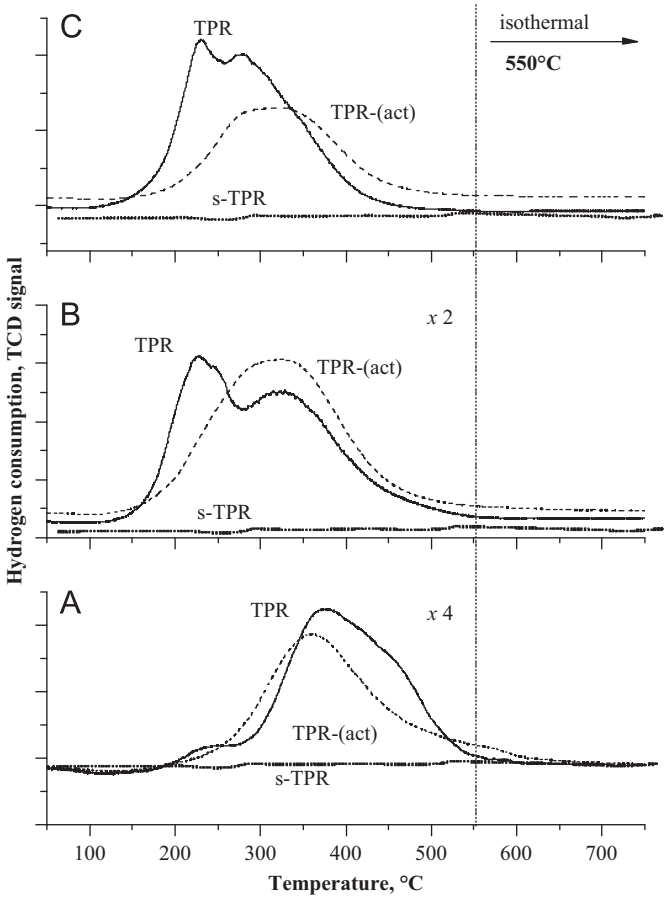

Fig. 4. TPR and TPR-(act) profiles of (*1.86*)Cu/Y (A), (*5.31*)Cu/Y (B) and (*8.22*)Cu/Y (C) samples. The intensities of TCD signals in (B) and (C) are multiplied by 2 and 4, respectively.

Table 3
Quantitative TPR results obtained on (x)Cu/Y and (x)Cu/Y-(act).

Cu content (x=*wt%*) *(ICP)*	*1.86*	*5.31*	*8.22*	*11.82*	*15.96*
Cu content (*mmol/g*) *(ICP)*	*0.29*	*0.84*	*1.29*	*1.87*	*2.51*
Hydrogen consumption experimentally obtained during TPR (mmol H_2/g) (h_1)	0.15	0.46	0.77	1.40	2.52
Hydrogen consumption experimentally obtained during s-TPR (mmol H_2/g)	0	0	0	0.03	0.02
Exposed surface Cu^0 detected by s-TPR (mmol/g)[a]	0	0	0	0.06	0.04
Hydrogen consumption experimentally obtained during TPR-(act) (mmol H_2/g) (h_2)	0.09	0.31	0.49	0.68	n.d.[d]
Hydrogen consumption experimentally obtained during s-TPR-(act) (mmol H_2/g)	0	0	0	0	n.d.[d]
Exposed surface Cu^0 detected by s-TPR-(act) (mmol/g)[a]	0	0	0	0	–
Portion of weakly stabilized Cu(II): $[(h_1)-(h_2)]/(h_1)$	0.36	0.33	0.37	0.52	–
Hydrogen consumption (mmol H_2/g) expected for reduction:					
Cu(II) to Cu(0)[b]	0.29	0.84	1.29	1.86	2.51
Cu(II) to Cu(I)[c]	0.15	0.42	0.65	0.93	1.26

[a] According to reaction (2).
[b] According to reaction (1).
[c] According to reaction (5).
[d] Not determined.

samples (x=*1.36, 4.55, 9.19*) are shown in Fig. 6. It can be seen that the reduction of (x)Cu/SAPO-5 samples with $x<5$ occurs in a broad temperature range between 150 and 550 °C. The broad reduction profile consists of at least two peaks, an LT peak at ca. 300 °C and a HT peak at ca. 400 °C. For samples containing higher Cu contents, the intensity of the LT peak becomes dominant and the reduction profile is narrowed. The argon pre-treatment diminishes the intensity of the LT peak similar to Cu/Y samples. However, unlike the Cu/Y samples, the s-TPR and s-TPR-(act) profiles of Cu/SAPO-5 and Cu/SAPO-5-(act), respectively, with Cu contents of $x \geq 1.36$ exhibit a hydrogen consumption at around 200 °C, indicating the existence of metallic Cu^0 after TPR. Fig. 7 depicts the experimental and expected amounts of hydrogen consumed during TPR calculated using Eq. (4) as a function of the total Cu content. It can be seen that the values of hydrogen consumption for the reduction of Cu in (x)Cu/SAPO-5 with $x<5$ correspond to the values expected for the change of oxidation state $n-m=1$. For (x)Cu/SAPO-5-(act) samples with $x<5$, however, there is a slight deviation to $n-m<1$ in this range of Cu loading, comparable to the Cu/Y-(act) samples. With increase in Cu content, Fig. 7 demonstrates, however, that the TPR hydrogen consumption obtained for both (x)Cu/SAPO-5 and (x)Cu/SAPO-5-(act) approaches the hydrogen consumption required for the change of oxidation state $n-m=2$, which is an analog to the reduction of (x)Cu/Al_2O_3, see Table 2 and Fig. 3.

To get further information on the state of Cu, XRD measurements were carried out for the (*6.53*)Cu/SAPO-5 sample (a) calcined at 400 °C for 4 h, (b) calcined as (a) and then reduced by TPR, (c) calcined as (a) and then activated in Ar at 650 °C for 12 h and (d) pre-treated as step (c) and thereafter reduced by TPR. The corresponding patterns are presented in Fig. 8. Unlike the TPR and s-TPR results of the sample (*6.53*)Cu/SAPO-5 (Table 4) indicating the

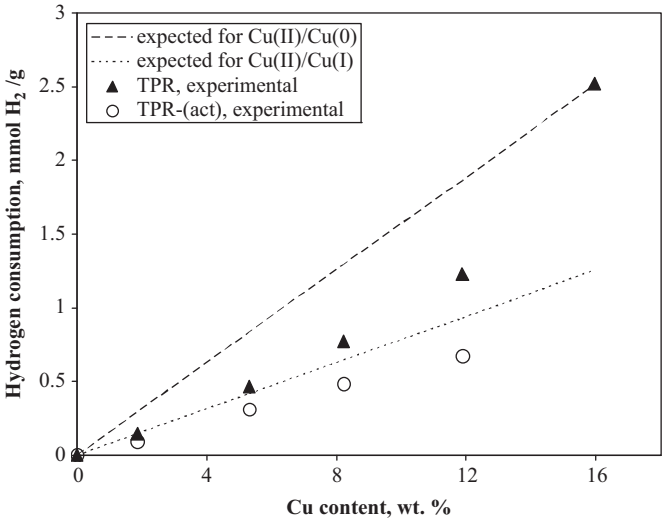

Fig. 5. Hydrogen consumption (mmol H_2/g) obtained by TPR and TPR-(act) in dependence on the Cu content (wt%.) of Cu/Y.

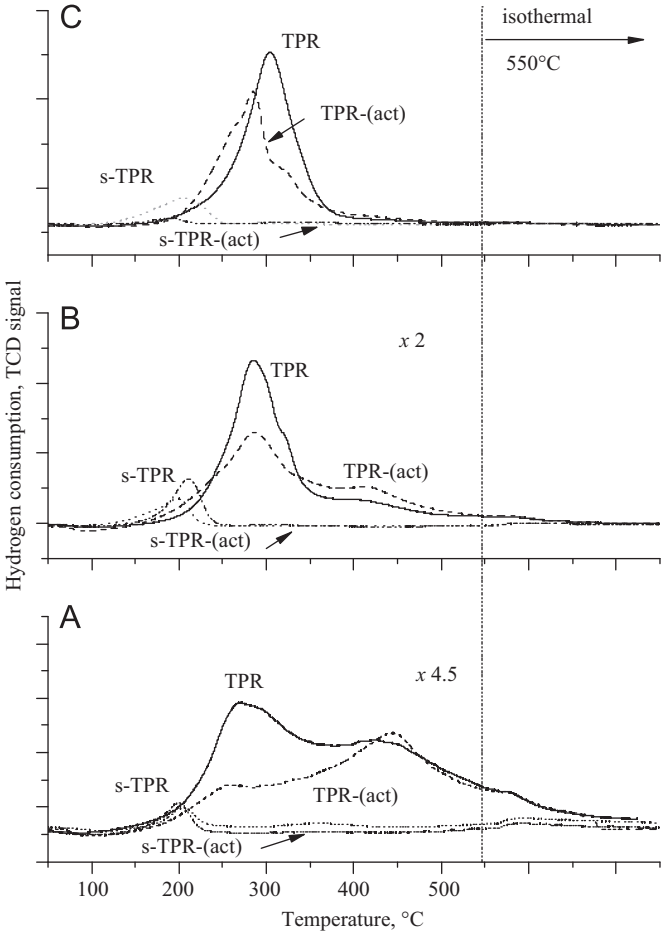

Fig. 6. TPR, TPR-(act), s-TPR and s-TPR-(act) profiles of (*1.36*)Cu/SAPO-5, (*4.55*)Cu/SAPO-5 and (*9.19*)Cu/SAPO-5 samples. The intensities of TCD signals in (B) and (C) are multiplied by 2 and 4.5, respectively.

Table 4
Quantitative TPR results obtained on (x)Cu/SAPO-5 and (x)Cu/SAPO-5-(act).

Cu content, x=(wt%) (ICP)	*0.78*	*1.36*	*2.26*	*4.55*	*6.53*	*9.19*
Cu content (mmol/g) (ICP)	*0.12*	*0.21*	*0.36*	*0.72*	*1.03*	*1.45*
Hydrogen consumption experimentally obtained during TPR (mmol H_2/g) (h_3)	0.07	0.12	0.23	0.49	0.88	1.46
Hydrogen consumption experimentally obtained during s-TPR (mmol H_2/g)	0	0.013	0.017	0.05	0.05	0.1
Exposed surface Cu^0 detected by s-TPR (mmol/g)[a]	0	0.026	0.034	0.1	0.1	0.2
Hydrogen consumption experimentally obtained during TPR-(act) (mmol H_2/g) (h_4)	0.04	0.07	0.12	0.33	0.61	1.21
Hydrogen consumption experimentally obtained during s-TPR-(act) (mmol H_2/g)	0	0	0.01	0.01	0.05	0.03
Exposed surface Cu^0 detected by s-TPR-(act) (mmol/g)[a]	0	0	0.02	0.03	0.1	0.07
Portion of weakly stabilized Cu(II) $[(h_3)-(h_4)]/(h_3)$	0.44	0.42	0.47	0.32	0.31	0.17
Hydrogen consumption (mmol H_2/g) expected for reduction:						
Cu(II) to Cu(0)[b]	0.12	0.2	0.36	0.72	1.03	1.45
Cu(II) to Cu(I)[c]	0.06	0.1	0.18	0.34	0.51	0.72

[a] According to reaction (2).
[b] According to reaction (1).
[c] According to reaction (5).

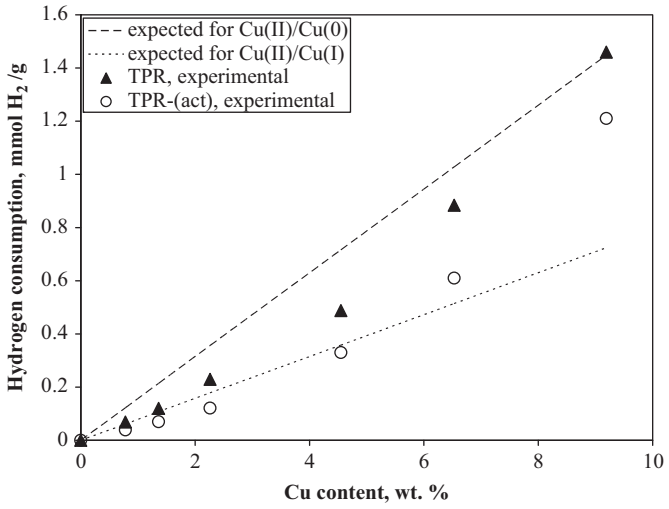

Fig. 7. Hydrogen consumption (mmol H_2/g) obtained by TPR in dependence on the Cu content (wt%.) of Cu/SAPO-5 and Cu/SAPO-5-(act).

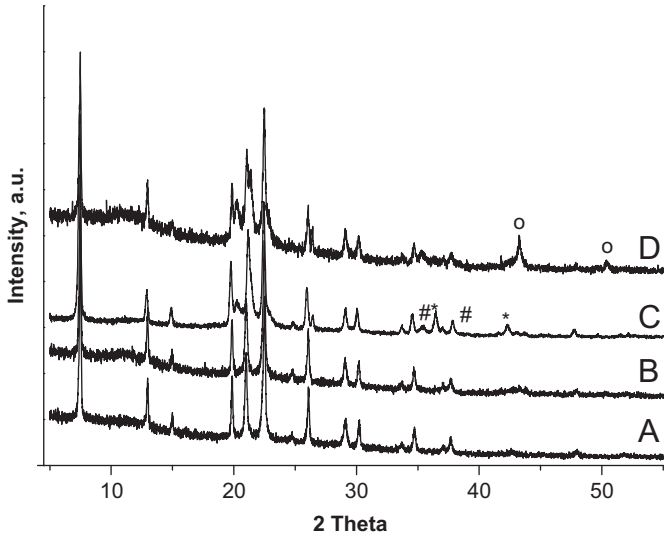

Fig. 8. XRD patterns of the sample (6.53)Cu/SAPO-5 (A) calcined at 400 °C for 4 h, (B) after TPR, (C) (6.53)Cu/SAPO-5-(act) and (D) after TPR-(act). (#)=CuO, (*)=Cu_2O and (o)=metallic Cu.

existence of CuO and Cu^0 on this sample before (a) and after reduction (b), respectively, the CuO and metallic Cu^0 phases are not observed in the corresponding XRD patterns. This gives the hint on a high dispersion of Cu species on SAPO-5 support. In contrast, XRD reveals, in agreement with TPR-(act) and s-TPR-(act) (Table 4), the existence of a mixture of Cu_2O and CuO (the XRD pattern c) and Cu^0 phases (the XRD pattern d). This indicates that the activation may cause an agglomeration of Cu species in Cu/SAPO-5.

The XPS Cu2*p* spectra of the samples (*6.53*)Cu/SAPO-5 and (*6.53*)Cu/SAPO-5-(act) are presented in Fig. 9, which shows the electron binding energies at 930.1 and 931.6 eV for the fresh and activated sample, respectively. The spectrum of the calcined sample exhibits the characteristic satellite bands of bivalent Cu at 940.1 and 959.7 eV, whereas the one of the activated sample does not. Without exhibiting these satellites, the spectrum (b) in Fig. 9 can evidence the absence of Cu^{2+} species [32,33]. The spectra of the CuLMM Auger peaks favor the existence of Cu^+ species for this activated sample and do not give any hints

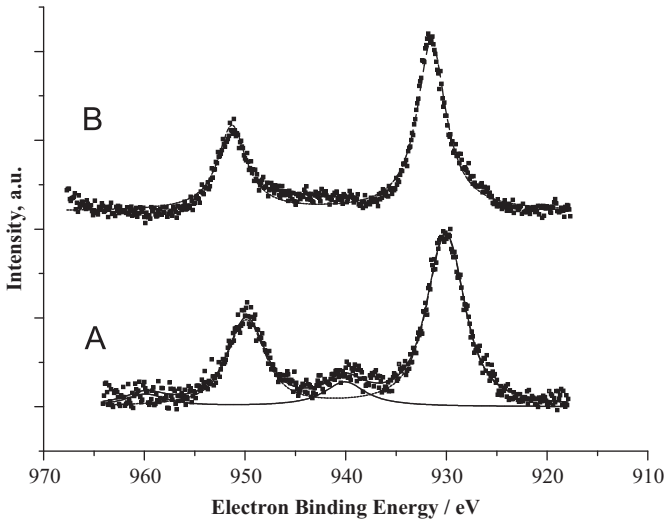

Fig. 9. XPS spectra of (*6.53*)Cu/SAPO-5 (A) and (*6.53*)Cu/SAPO-5-(act) (B).

for metallic Cu. It is remarkable that a lower binding energy was detected at the calcined sample than at the activated one, which seems to be in contrast to the existence of the satellites. The Cu peaks at the calcined sample are significantly broader than at the activated sample, suggesting a higher heterogeneity of the Cu sites at this sample. But, a further deconvolution of the Cu peak at the calcined sample is not reasonable. This conclusion is, on the one hand, it is only valid for the near-surface regions of bulk materials depending on the range of penetration depth of photoelectrons. But, on the other hand, this is in agreement with TPR and XRD results presented above, revealing the existence of Cu^+ after the activation in argon.

4. Discussion

In the form of powders as well as supported on alumina or in mixture with other oxides, Cu oxides are reduced by hydrogen either in one step directly to metallic Cu^0 according to reaction (1) [6,11,22,25–27] or sequentially according to reaction (5) and then (2):

$$2CuO + H_2 \rightarrow Cu_2O + H_2O \quad (5)$$

Because the reduction of Cu_2O is more difficult than the reduction of CuO, reaction (1) is found to be dominant at lower temperatures $<300^{\circ}C$, whereas the reactions (2) and(5) are favored at higher temperatures [25]. Moreover, at high temperatures and very low pressures of O_2 and/or under vacuum, the auto-reduction reaction (6) of CuO may take place [26]:

$$2CuO \rightarrow Cu_2O + 0.5O_2 \quad (6)$$

In the case of Cu supported on Al_2O_3, on the one hand, the appearance of hydrogen consumption peaks in the s-TPR profiles, see Fig. 2, evidences the existence of metallic Cu^0, i.e. the final oxidation state $m=0$ (see Eq. (4)) on the Cu/Al_2O_3 and Cu/Al_2O_3-(act) samples after the first TPR run. On the other hand, Fig. 3A demonstrates that the total change of oxidation state is $n-m=2$ for $(x)Cu/Al_2O_3$ and $n-m=1$ for $(x)Cu/Al_2O_3$-(act) at $x<6.42$. This leads to the conclusion that the initial oxidation states of Cu in $(x)Cu/Al_2O_3$ and $(x)Cu/Al_2O_3$-(act) samples should be $n=2$ and $n=1$, respectively.

This can be explained referring to reactions (1), (5) and (6). Thus, at $x<6.42$, the reduction of $(x)Cu/Al_2O_3$ samples seem to

occur according to reaction (1) in one step, i.e. only one peak is observed in the TPR profiles (see Fig. 2). The appearance of the second reduction peak in the reduction profile of (*8.47*)Cu/Al_2O_3 suggests the two-step reduction according to reactions (5) and (2), where the first peak might be assigned to reaction (5) and the second one to reaction (2). Although it is not shown here, the appearance of further reduction peaks in the TPR profiles can be observed for (*x*)Cu/Al_2O_3 samples at $x>8$. During the high temperature pre-treatment in argon, auto-reduction (reaction (6)) had taken place so that all the available Cu^{2+} cations in the samples with $x<6.42$ are almost quantitatively transformed into Cu^{+}. These Cu^{+} ions can further be reduced by hydrogen to Cu^0 according to reaction (2). However, at $x>6.42$, the argon pre-treatment does not affect the reduction of Cu as shown in Fig. 3A. This indicates that the auto-reduction (6) in argon at 650 °C probably does not take place with the samples containing high contents of Cu oxides.

The amount of Cu^0 detected by s-TPR and s-TPR-(act) for (*x*)Cu/Al_2O_3 and (*x*)Cu/Al_2O_3-(act) samples, respectively, linearly increases with increase in the total Cu content up to 6.42 wt% (1.0 mmol Cu/g), see Fig. 3B. This means the ratios of exposed surface Cu^0 detected by s-TPR or s-TPR-(act) to the total Cu are stable, hinting on a high and stable dispersion of Cu species in this range of Cu content. The drastic decrease of the hydrogen consumption at higher Cu contents (> 1.0 mmol Cu/g) indicates, therefore, the decrease in Cu dispersion that can be caused by a strong agglomeration of Cu species. Such strongly agglomerated state may be the reason why the auto-reduction of Cu oxides in argon did not proceed to a noticeable extent.

The s-TPR experiments on (*x*)Cu/Y and (*x*)Cu/Y-(act) samples, as shown in Table 3, reveal the absence of Cu^0 in the samples at $x<8$ after TPR. Further, Fig. 5 demonstrates that the total change of the Cu oxidation state is $n-m=1$ for these (*x*)Cu/Y samples. This suggests that the initial oxidation state *n* of Cu supported on zeolite Y at Cu contents < 8 wt% should be 2+ and the final oxidation state after TPR according to reaction (5) should be 1+. This finding disagrees with the reduction mechanism leading to Cu^0 as the final state reported in [3,34,35]. But, it is in agreement with the results reported in [12] that Cu^{+} can be stabilized by Y support so that it cannot be reduced further to form Cu^0. In this case, the hydrogen consumption in s-TPR would be 0 and the Cu dispersion, as defined in [15–17], would be erroneously 0 as well.

The fact that the TPR profiles of the calcined (*x*)Cu/Y samples show at least two reduction peaks can be explained by referring to the existence of Cu species located at different positions within the faujasite structure of zeolite Y. Actually, it has been discussed a variety of Cu species may exist in zeolites, comprising isolated Cu cations at ion-exchange positions, O-bridged Cu dimers $[Cu\text{-}O\text{-}Cu]^{2+}$ or even chains, Cu^0 nanocluster, as well as crystalline Cu, Cu_2O and CuO of different sizes [3,34–38]. According to this variety, complex reduction profiles are normally observed. Further, as described above, the LT peaks in TPR profiles of Cu/Y samples vanished after pre-treatment by argon (see Fig. 4) and the hydrogen consumption decreases accordingly (see Table 3 and Fig. 5). This gives evidence that Cu^{2+} species anchored within Y zeolite should be differently stabilized against reduction. The weakly stabilized Cu^{2+} species can either be reduced by hydrogen at T_{max} of ca. 250 °C (this corresponds to the LT peak) or auto-reduced in argon at 650 °C according to reaction (6) or according to the mechanisms of the reduction of Cu ions during thermovacuum treatment described by Chen et al. [38], forming Cu^{+}. In contrast to this, the strongly stabilized Cu^{2+} cations are reduced only by hydrogen yielding the HT peak and do not suffer auto-reduction in argon. Hence, the hydrogen consumed for reduction of (*x*)Cu/Y-(act) would quantitatively correspond to the amount of Cu^{2+} strongly stabilized. The difference between hydrogen consumed for reduction of (*x*)Cu/Y, designated as (h_1), and (*x*)Cu/Y-(act), designated as (h_2), would be equal to the amount of weakly stabilized Cu^{2+} cations. The portion of weakly stabilized Cu^{2+} cations, $[(h_1)-(h_2)]/(h_1)$, slightly increases with increase in Cu content (see Table 3). At higher Cu content, $x>8$, the formation of Cu^0 after TPR is detected by s-TPR while the amounts of weakly stabilized Cu^{2+} cations and the $(n-m)$ values increase, approaching $(n-m)=2$, see Table 3. This indicates that a portion of Cu^{2+} weakly stabilized on zeolite Y may be directly reduced by hydrogen to Cu^0 according to reaction (1) [3,34,35].

The reduction behavior of Cu^{2+} in (*x*)Cu/SAPO-5, at $x<5$, seems to be similar to the reduction of Cu^{2+} in Cu/Y. This similarity suggests that in this range of Cu contents, Cu^{2+} species are initially also differently, weakly and strongly, stabilized within the SAPO-5 structure against the reduction. The weakly stabilized Cu^{2+} can either be reduced by hydrogen at low temperature or transformed under argon at 650 °C (reaction (6)) into Cu^{+} [26,28]. Similar to the strongly stabilized Cu cations in Cu/Y, the strongly stabilized Cu^{2+} cations in Cu/SAPO-5 are also reduced only by hydrogen causing the HT peak, and they do not suffer from auto-reduction in argon. Like the case of Cu/Y, the hydrogen consumption obtained in s-TPR of Cu/SAPO-5 samples, reduced by TPR and followed by a N_2O reoxidation, would be either 0 or very low and, therefore, could not be used for calculation of the Cu dispersion.

Possible locations of Cu^{2+} cations in the AFI structure of SAPO-5 have been discussed by Chen and Kevan [39], Lee et al. [40] and Hartmann and Kevan [41]. In earlier works [23], some problems concerning the possible locations of Cu ions as isolated, O-bridged dimers or isomorphously substituted into the framework have been discussed based on FTIR, XPS, XRD and TPR results. At this stage of studies, only by means of TPR measurements, it is difficult to make an assignment for the location of weakly and strongly stabilized Cu^{2+} species. In analogy to the discussion given above for Cu/Y samples, the hydrogen consumed for reduction of (*x*)Cu/SAPO-5-(act), with $x<5$, would quantify the amount of strongly stabilized Cu^{2+} and the difference between hydrogen consumed for reduction of (*x*)Cu/SAPO-5, designated as (h_3), and (*x*)Cu/SAPO-5-(act), designated as (h_4), would give the amount of weakly stabilized Cu^{2+} cations on SAPO-5. Based on the data presented in Table 4, the portion of weakly stabilized Cu^{2+}, $[(h_3)-(h_4)]/(h_3)$, can be estimated. With increase in Cu content, the results presented in Fig. 7 show that the reduction of Cu in Cu/SAPO-5 becomes similar to the reduction of Cu in Cu/Al_2O_3 (Fig. 3A). This suggests that the mechanism of Cu^{2+} reduction changes and the reactions (1) and/or (5) and (2) may become dominant so that the product of reduction is predominantly metallic Cu^0. This may also be the reason explaining why the portion of Cu^{2+} weakly stabilized against an auto-reduction in argon, $[(h_3)-(h_4)]/(h_3)$, decreases with increase in Cu content (Table 4).

The differences observed above in the reduction behavior of Cu supported on Al_2O_3, zeolite Y and SAPO-5 are certainly correlated with the different natures of supports. The different texture and the surface functionality of Al_2O_3, zeolite Y, and SAPO-5 account for the variety of Cu species formed during the impregnation process. Al_2O_3 does not possess strong acid sites, therefore, Cu^{2+} and/or Cu^{+} ions can only be stabilized on this support by embedding into an aluminate matrix [6]. In contrast, zeolite Y and SAPO-5 have strong acid sites that are responsible for anchoring Cu ions. Zeolite Y exhibits three building parts of the structure, viz. the supercage, the sodalite units and the hexagonal prisms where single Cu ions can be anchored to the framework [12,36,37]. The pore structure of SAPO-5 is characterized by parallel arranged main pores of 0.7 nm size where strong acid sites, including Brønsted ones, are located. But, Brønsted acid sites

also exist in structural subunits, as recognizable by ^{1}H MAS NMR spectroscopy [42]. It can be expected that the stabilization of Cu in zeolite Y and SAPO-5 is effective as long as the strong acid sites, as shown in Table 1, amount to ca. 1.9 mmol/g for zeolite Y, see [12], and ca. 0.7 mmol/g for SAPO-5 are available. Once the loading exceeds these limits, i.e. 1.9 mmol Cu/g (equivalent to ca. 12 wt%) for zeolite Y and 0.7 mmol Cu/g (equivalent to ca. 4.2 wt%) for SAPO-5, Cu agglomeration is unavoidable. This estimation can be used to explain the TPR results obtained for (x)Cu/Y and (x)Cu/SAPO-5. As appeared, there exists a limit with $x>8$ for Cu/Y and $x>5$ for Cu/SAPO-5 where portions of Cu species are reduced to Cu^0 as shown by s-TPR and XRD measurements. This suggests that, at these ranges of Cu loading, CuO agglomerates may be formed and the reduction occurs more and more according to reaction (1). As shown by XPS, however, this does not exclude the existence of Cu^+ on the surfaces due to auto-reduction leading to the $(n-m)$ values <2.

5. Conclusions

The TPR and s-TPR experiments reveal different reduction behaviors of Cu supported on Al_2O_3, zeolite Y and SAPO-5. The quantitative results show that the initial oxidation state of Cu after calcination in air at 400 °C is predominantly +2, independent of the nature of the support.

Supported on Al_2O_3, Cu^{2+} is shown to be quantitatively reduced to Cu^0 by H_2. A treatment of (x)Cu/Al_2O_3, with $x<7$, in argon at 650 °C induces an auto-reduction and transforms almost quantitatively all available Cu^{2+} into Cu^+ that is further reduced to Cu^0 by H_2. In this range of Cu contents, Cu species are shown to be highly dispersed on the Al_2O_3 support. The argon pre-treatment of the Cu/Al_2O_3 samples containing more than 7 wt% Cu does not cause auto-reduction and the reduction of Cu in these cases occurs according to reactions (1), (2) and (5). This indicates a highly agglomerated state of Cu in the form of CuO.

For (x)Cu/Y, with $x<8$, TPR experiments enable one to distinguish Cu^{2+} species as weakly and strongly stabilized against an auto-reduction in argon at 650 °C. The weakly stabilized Cu^{2+} species could be shown to become reduced either by H_2 at low temperatures (ca. 250 °C) or auto-reduced under argon pre-treatment at 650 °C to form Cu^+. The percentage of the weakly stabilized Cu^{2+} remains unchanged at ca. 30–40% if the Cu content x is less than 8 wt%, and increases with increase in Cu content.

The reduction of Cu^{2+} in (x)Cu/SAPO-5 with $x<5$ shows similarities to the reduction of Cu^{2+} in Cu/Y, i.e. Cu^+ is formed but cannot be further reduced to Cu^0 under the TPR experimental conditions. In this range of Cu loading, Cu^{2+} species, weakly and strongly stabilized against auto-reduction in argon, are present. The weakly stabilized Cu^{2+} species are reduced by H_2 at low temperature or transformed by argon pre-treatment at 650 °C into Cu^+. The percentage of the weakly stabilized Cu^{2+} is estimated to amount to 40–50%. This portion decreases with increase in Cu content ($x>3$). This may be reasoned by an agglomeration of weakly stabilized Cu^{2+} ions to CuO_x and a change of the reduction mechanism of Cu^{2+} on (x)Cu/SAPO-5 leading to the formation of metallic Cu^0 as in the case of (x)Cu/Al_2O_3, with $x>7$ wt%.

The definition of Cu dispersion as a ratio of hydrogen consumed in s-TPR to hydrogen consumed in TPR can only be applied to the cases of (x)Cu/Al_2O_3, where Cu oxides are shown to be reduced to metallic Cu^0. Supporting on zeolite Y or SAPO-5, a portion of Cu^+ ions can be fixed on acid sites, i.e. highly dispersed, even at an atomic level, without any formation of Cu^0. In this case, using s-TPR, the hydrogen consumption would be either 0 or very low, so that the Cu dispersion, as defined above, would be erroneously 0 or very low, respectively.

Acknowledgment

Thi Thuy Hanh Dang gratefully acknowledges grants from the Government of S.R. Vietnam, the Deutscher Akademischer Austausch Dienst, DAAD, and LIKAT. Jana Engeldinger gratefully acknowledges grants from the Deutsche Forschungsgemeinschaft, DFG (RI 829/7-1) and LIKAT. Mrs. W. Winkler and Mr. R. Eckelt are thanked for the XRD and N_2 adsorption measurements.

References

[1] S.D. Robertson, B.D. McNikol, J.H. de Baas, S.C. Kloet, J.W. Jenkins, J. Catal. 37 (1975) 424–431.
[2] J.W. Jenkins, B.D. McNicol, S.D. Robertson, Chem. Tech. 7 (1977) 316–320.
[3] S.J. Gentry, N.W. Hurst, A. Jones, J. Chem. Soc. Faraday Trans. 1 (75) (1979) 1688–1699.
[4] A. Jones, B.D. McNicol, TPR for Solid Materials Characterization, Marcel Dekker, Inc., New York-Basel, 1986.
[5] A. Wöllner, F. Lange, H. Schmelz, H. Knözinger, Appl. Catal. A: General 94 (1993) 181–203.
[6] M. Fernández-García, I. Rodrigez-Ramos, P. Ferreira-Aparacio, A. Guerro-Ruiz, J. Catal. 178 (1998) 253–263.
[7] R. Bulánek, B. Wichterlová, Z. Zobalík, J. Tichý, Appl. Catal. B: Environ. 31 (2001) 13–25.
[8] P. Da Costa, B. Moden, G.D. Meitzner, D.K. Lee, E. Iglesia, Phys. Chem. Chem. Phys. 4 (2002) 4590–4601.
[9] J. Sárkány, J.L. dĬtri, W.M.H. Sachtler, Catal. Lett. 16 (1992) 241–249.
[10] W.-P. Dow, Y.-P. Wang, T.-J. Huang, J. Catal. 160 (1996) 155–170.
[11] M.M. Günter, T. Ressler, R.E. Jentoft, B. Bems, J. Catal. 203 (2001) 133–149.
[12] M. Richter, M.J.G. Fait, R. Eckelt, M. Schneider, J. Radnik, D. Heidemann, R. Fricke, J. Catal. 245 (2007) 11–24.
[13] M. Richter, M.J.G. Fait, R. Eckelt, E. Schreier, M. Scneider, M.-M. Pohl, R. Fricke, Appl. Catal. B: Environ. 73 (2007) 269–281.
[14] C.M. Chanquía, K. Sapag, E. Rodrígez-Castellon, E.R. Herrrero, G.A. Eimer, J. Phys. Chem. C 114 (2010) 1481–1490.
[15] S. Sato, R. Takahashi, T. Sodesawa, K. Yuma, Y. Obata, J. Catal. 196 (2000) 195–199.
[16] A. Gervasini, S. Bennici, Appl. Catal. A 281 (2005) 199–205.
[17] E.D. Guerreiro, O.F. Gorriz, G. Larsen, L.A. Arrúa, Appl. Catal. A 204 (2000) 33–48.
[18] M. Hartmann, L. Kevan, Res. Chem. Intermed. 28 (7–9) (2002) 625–695.
[19] G. Genti, S. Perathoner, Appl. Catal. A 132 (1995) 179–259.
[20] K. Mathisen, D.G. Nicholson, M. Stockenhuber, Micropor. Mesopor. Mater 84 (2005) 261–274.
[21] A. Dandekar, M.A. Vannice, J. Catal. 178 (1998) 621–639.
[22] F.E. López-Suárez, A. Bueno-López, M.J. Illán-Gómez, Appl. Catal. B 84 (2008) 651–658.
[23] T.T.H. Dang, H.-L. Zubowa, U. Bentrup, M. Richter, A. Martin, Micropor. Mesopor. Mater 123 (2009) 209–220.
[24] D.L. Hoang, H. Lieske, Thermochim. Acta 345 (2000) 93–99.
[25] J.A. Rodriguez, J.Y. Kim, J.C. Hanson, M. Pérez, A.I. Frenkel, Catal. Lett. 85 (3–4) (2003) 247–254.
[26] J.Y. Kim, J.A. Rodriguez, J.C. Hanson, A.I. Frenkel, P.L. Lee, J. Am. Chem. Soc. 125 (2003) 10684–10692.
[27] T.L. Reitz, P.L. Lee, K.F. Czaplewski, J.C. Lang, K.E. Popp, H.H. Kung, J. Catal. 199 (2001) 193–201.
[28] A.M. Monti, A. Baiker, J. Catal. 83 (1983) 323–335.
[29] M. Richter, B. Parlitz, R. Eckelt, R. Fricke, Chem. Commun. (1997) 383–384.
[30] C. Halik, J.A. Lercher, H. Mayer, J. Chem. Soc., Faraday Trans. 1 84 (12) (1988) 4457–4469.
[31] E. Gianotti, E.C. Oliveira, S. Coluccia, H.O. Pastore, L. Marchese, Inorg. Chim. Acta 349 (2003) 259–264.
[32] G. Ertl, R. Hierl, H. Knözinger, N. Thiele, H.P. Urbach, Appl. Surf. Sci. 5 (1980) 49–64.
[33] L. Meda, G.F. Cerofolini, Surf. Interface Anal. 36 (2004) 756–759.
[34] S. Kieger, G. Delahay, B. Coq, B. Neveu, J. Catal. 183 (1999) 267–280.
[35] M. Afza, G. Yasmeen, M. Saleem, J. Afzal, J. Therm. Anal. Calorim. 62 (2000) 277–284.
[36] A. Delabie, K. Pierloot, M.H. Groothaer, R.A. Schoonheydt, L.G. Vanquickenborne, Eur. J. Inorg. Chem. (2002) 515–530.
[37] I.J. Drake, Y. Zhang, D. Briggs, B. Lim, T. Chau, A.T. Bell, J. Phys. Chem. B 110 (2006) 11654–11664.
[38] H. Chen, M. Matsuoka, J.J. Zhang, M. Anpo, J. Catal. 228 (2004) 75–79.
[39] X. Chen, L. Kevan, J. Am. Chem. Soc. 113 (1991) 2861–2865.
[40] Ch.W. Lee, X. Chen, L. Kevan, Catal. Lett. 15 (1992) 75–81.
[41] M. Hartmann, L. Kevan, Chem. Rev. 99 (3) (1999) 635–663.
[42] B. Zibrowius, E. Löffler, M. Hunger, Zeolites 12 (1992) 167–174.